Targeting Efficiency and Biodistribution of Zoledronate Conjugated Docetaxel Loaded Pegylated PBCA Nanoparticles for Bone Metastasis

*Kiran R. Chaudhari, Abhinesh Kumar, Vinoth Kumar Megraj Khandelwal, Anil K. Mishra, Jukka Monkkonen, and Rayasa S. Ramachandra Murthy**

In an attempt to improve tumor localization of docetaxel (DTX)-loaded nanoparticles (NPs), zoledronic acid (ZOL) is used as a ligand to target bone metastasis. DTX-loaded ZOL-conjugated polyethylene glycol (PEG) ylated polybutyl cyanoacrylate (PBCA) NPs are prepared using an anionic polymerization technique. PBCA-PEG-ZOL NPs are subjected to cytotoxic assay in both BO2 and MCF-7 cell lines. Cell cycle arrest and apoptosis induced by the PBCA-PEG-ZOL NPs are studied. Quantitative cellular uptake, NP uptake route characterization, confocal microscopy and IPP/ApppI levels are performed. PBCA-PEG-ZOL NPs show an enhanced cytotoxic effect in both BO2 as well as MCF-7 cell lines due to higher uptake following ZOL-mediated endocytosis. The molecular basis of apoptosis reveals the involvement of a cytoplasmic protein in activating the programmed cell death pathway. Route characterization studies reveal that PBCA-PEG-ZOL NPs uptake is not completely blocked even by using both inhibitors (genistein and phenyl arsinoxide) simultaneously, conferring that uptake is not entirely based upon clathrin or caveolae. PBCA-PEG-ZOL NPs showed 7 and 5.3 times increase in IPP and ApppI production, in comparison to ZOL treatment, and 138 times higher than the control group in MCF-7 cell line. In BO2 cell line, after treatment with NPs, IPP was 5.35 times higher than ZOL solution. No ApppI in BO2 cell line after treatment with NPs and ZOL solution was found. NP distribution in tumor infected bone is also significantly high in comparison to the normal bone at any time point. It is concluded that ZOL-conjugated NPs provide an efficient and targeted delivery of DTX, with synergistic effects. Thus, these NPs present a promising treatment in the near future, by actively targeting metastatic tumor.

1. Introduction

The deadliest characteristic of a cancerous cell is its ability to metastasize. Bone is the most common site of metastasis for various types of cancers. About, 70% of patients suffering from advanced prostate or breast cancer, develop bone metastasis. Although bone metastases are incurable, patients have mean survival of several years, as nearly 40% of those with breast cancer bone metastases survive for five years.[1]

Various complications which may be noticeable in bone metastases are osteolysis, spinal cord compression, hypercalcemia, increased fracture incidence and unrelenting pain.[2] There are very rare chances for patients to be cured after bone metastasis. Thus, prevention of metastasis is the only approach to improve the survival rate of the patient, and hence, the quality of life. However, partial understanding of the metastasis has slowed down any development in this regard emphasizing metastasis.[3] One disadvantage of the conventional therapy is the inability to achieve the desired concentration at bones, to suppress tumor. An ideal chemotherapeutic system should specifically target the cancer cells in bone marrow, resulting in cytotoxicity to malignant cells, particularly for the treatment of

Dr. K. R. Chaudhari, Dr. A. Kumar
TIFAC Centre of Relevance and Excellence in New Drug Delivery Systems
Shri G. H. Patel Pharmacy Building
Pharmacy Department
The Maharaja Sayajirao University of Baroda
Donor's Plaza, Fatehgunj, Vadodara-390002, India
Dr. K. R. Chaudhari, Dr. V. K. M. Khandelwal, Prof. J. Monkkonen
School of Pharmacy, Faculty of Health Sciences
University of Eastern Finland, Kuopio-70211, Finland
Dr. K. R. Chaudhari, Dr. A. K. Mishra
Department of Radiopharmaceuticals and Radiation Biology
Institute of Nuclear Medicine and Allied Sciences (INMAS)
Brigadier S. K. Mazumdar Road, Delhi-110054, India
Dr. V. K. M. Khandelwal
Tumor Cell Invasion Laboratory
Consorzio Mario Negri Sud, Santa Maria Imbaro-66030, Italy
Prof. R. S. R. Murthy
ISF College of Pharmacy, Firozpur G. T. Road, Moga-142001, Punjab, India
E-mail: m_rsr@rediffmail.com

DOI: 10.1002/adfm.201102357

bone metastasis. Delivery system of drug conjugates that exploit the concept of tissue or cellular selectivity using bisphosphonate (BP), to target metastatic bone cancer is reported by El-Mabhouha et al.[4] Several attempts have already been made to use bisphosphonates to deliver chemotherapy or radiotherapy based on their affinity to the bone.[5] One of such approaches for targeting the bone involves the development of an osteotropic alendronate-b-cyclodextrin conjugate (ALN-b-CD), which can form inclusion complex with prostaglandin E1 (PGE1, a potent bone anabolic agent), for improved treatment of skeletal diseases. In a bilateral rat mandible model, ALN-b-CD/PGE1 molecular complex was found to stimulate a strong local bone anabolic reaction.[6] In another effort, a new bisphosphonate (BP) derivative cholesteryl trisoxyethylenebisphosphonic acid (CHOL-TOE-BP) was used as bone targeting moiety for liposomes, due to the exceptional affinity of bisphosphonates for hydroxyapatite. In vitro data suggested that this carrier may be useful as a targeting device for liposomal drug delivery to the bone.[7] Bone targeted polyethylene glycol (PEG) based system for the delivery of growth factors for the intent of bone repair is patented by Celtrix Pharmaceuticals.[8] A similar design of bisphosphonate based PEG delivery system targeting bone is patented by Nektar, in which one end of PEG is modified with bisphosphonate and other with drug. However, the drug release mechanism is still not clear.[9] Despite excellent targeting ability, no report is available for detailed in vivo studies to exploit bisphosphonate as a targeting ligand, using nanocarrier delivery system.

Previously, the pharmacokinetic study of C^{14}-labeled zoledronic acid (ZOL) in the rat and dog, showed a rapid and multiphasic post infusion decrease in plasma concentration, followed by prolonged very low levels. More than 100 fold concentration of ZOL was observed shortly after the infusion, and declined by some extent at six-months post dose. There was no evidence of any biotransformation of ZOL, and elimination was found to occur exclusively via the kidneys. The renal excretion quantified to about 40, 50, and 60% of the administered dose after 24 h, 6 and 12 months, respectively.[10]

Therefore, it is hypothesized that the proposed ZOL functionalized docetaxel (DTX) loaded nanoparticulate system may target bone metastasis with synergistic effect on metastatic tumor, thereby reducing bone complication by controlling osteoclast activity (by bisphosphonate), along with reduction in further metastasis by reducing activation of growth factors (by controlling osteoclast activity) and occult tumor cell count in blood.

2. Materials and Methods

2.1. Materials

Butylcyanoacrylate monomer was obtained as a gift sample from Evobond, Tong Shen Enterprise, Taiwan. DTX and ZOL were obtained as a gift sample from Sun Pharma Advanced Research Centre (SPARC), Vadodara, India. PEG bisamine (Mol wt. 3350 Da), N,N′-Carbonyldiimidazole (CDI), N-hydroxy succinimide (NHS) and 6-coumarin were purchased from Sigma Aldrich, India. Poloxamer 188 was kindly gifted by BASF, India. HCl, NaOH, SDS, DMF and DMSO were obtained from S. D. Fine Chemicals, India. MCF-7 cell line was obtained from ECACC (Salisbury, UK), RAW264 cell line was obtained from ATCC (USA), and BO2 cell line from INSERM, Research Unit 664, IFR62, Faculte de Medicine Laennec, Lyon, France. DMEM 21885, DMEM 31885, FBS, PBS, penicillin, streptomycin, trypsin, EDTA, and HBSS were purchased from GIBCO, Finland. RPMI 1640 was purchased from Lonza, Finland. 3-(4,5-Dimethylthiazol-2-yl)-2,5-diphenyltetrazolium bromide (MTT) and propidium Iodide (PI), stannous chloride dihydrate ($SnCl_2.2H_2O$) were purchased from Sigma Chemicals, USA. Tissue culture plates and flasks were purchased from NUNC, Denmark. Hoechst 33342 and RNAse A was purchased from Invitrogen, UK. Annexin V-FITC and binding buffer was purchased from Biolegend, USA. Sodium pertechnetate, separated from molybdenom-99 (99m) by solvent extraction method, was provided by Regional Center for Radiopharmaceutical Division (Northern Region), Board of Radiation and Isotope Technology (BRIT), Delhi, India.

2.2. Conjugation of ZOL with PEG Bisamine

Conjugation of ZOL with PEG bisamine was performed using CDI as a conjugation linker.[11] In brief, ZOL (100 mg) was dissolved in distilled DMF with triethylamine (TEA). CDI (90 mg, moisture-free) was added to the solution in a tightly closed vessel under a nitrogen blanket. The reaction mixture was allowed to react for 24 h at 60 °C on oil bath with constant stirring. TEA was evaporated on rotary flask evaporator to precipitate activated ZOL, which was separated by centrifugation. The precipitate was washed twice with acetonitrile to remove CDI and dried on rotary flask evaporator to obtain pure activated ZOL. PEG bisamine (1 g) and activated ZOL (22.6 mg) were dissolved in DMSO with TEA in a tightly closed vessel under nitrogen blanket and allowed to react for 12 h. Pure conjugate was separated using column chromatography using acetonitrile with TEA as mobile phase. The conjugate solution was dried on rotary flask evaporator, and stored in refrigerated conditions until further use. Each reaction step as well as the purification steps were monitored by TLC using acetonitrile:methanol (1:1), with TEA (1–2 drops) as a mobile phase and iodine as a spotting reagent. Conjugation of ZOL with PEG bisamine was confirmed by FTIR and NMR.

2.3. Preparation of NPs

2.3.1. Preparation of PBCA NPs

Polybutyl cyanoacrylate (PBCA) nanoparticles (NPs) were prepared by modified anionic polymerization technique as described previously.[12] Briefly, NPs were prepared in an acidic polymerization medium (pH 1.5-3) containing poloxamer 188 as a stabilizer. Double distilled water, filtered through 0.22 μm filter (Millipore, India) was used, which exhibited very low conductivity value. To the prepared aqueous acidic polymerization medium, monomer was added and probe sonicated for 2 min (100 W, 80% amp), followed by constant magnetic stirring at

700 rpm at 4 °C protected from light. The polymerization reaction was allowed to continue with stirring for 5 h. To complete the reaction, NaOH (0.5 M) was added until pH 5 and stirring was continued for a further 30 min. The NP suspension was then neutralized with NaOH (0.5 M), filtered through 0.4 μm filter (Millipore, India), separated by centrifugation (Sigma 3K30, Germany) and lyophilized (Heto Drywinner, Denmark) using trehalose as a cryoprotectant. In case of DTX and 6-coumarin loaded NPs, the respective material was dissolved in the monomer before adding into the polymerization media.

2.3.2. Preparation of PBCA-PEG NPs and PBCA-PEG-ZOL NPs

PBCA-PEG NPs were prepared in the similar manner as that of PBCA NPs with the addition of mPEGamine, and PBCA-PEG-ZOL NPs were prepared by using ZOL-PEG-amine as an initiator in the acidic polymerization medium. Amine group of PEG acts as a nucleophilic initiator of polymerization reaction, and propagated by the micellar emulsification process while later turn to NP formation.

2.4. Estimation of Entrapment Efficiency and Drug Loading

Lyophilized NPs (5 mg) were dissolved in 5 ml acetonitrile. The content of DTX was estimated using reverse phase HPLC (Shimadzu, Japan), with C18 column and acetonitrile:water (70:30) as mobile phase, 1 ml/min flow rate and ultraviolet detection at 230 nm. The percentage entrapment efficiency was calculated as a ratio of the total entrapped DTX to the total amount of DTX added.

2.5. In Vitro Cell Culture Studies

The mouse macrophage RAW 264 cell line and the human breast cancer MCF-7 cell line were maintained in DMEM-GLUTMAX and RPMI 1640 media, respectively. BO2 cell line, a sub-clone of MDA-MB-231, derived after six in vivo passages in nude mice and characterized by its unique morphology and affinity resembling to bone metastasis, was maintained in MEM-GLUTMAX.[13] The media was supplemented with 10% FBS, 100 U ml^{-1} penicillin, and 100 μg ml^{-1} streptomycin (Invitrogen, Paisley, UK). The cell lines were cultured at 37 °C in a 5% CO_2 humidified incubator.

2.5.1. In Vitro Bone Binding Assay, Quantitative Cell Uptake, Confocal Microscopy, and NPs Uptake Route Characterization

ZOL solution and PLGA-PEG-ZOL NPs were evaluated for in vitro bone binding affinity.[7] Both samples with an equal amount of ZOL were diluted with PBS, and kept on slow stirring along with the human simulated bone–hydroxyapatite powder, and binding was estimated at different time intervals. Cells were seeded on 6-well plates at the density of 1×10^5 cells per well and allowed to attach and grow. After 48 h, cells were incubated with 1 ml, 100 μg/ml 6-coumarin loaded PBCA-PEG NPs and PBCA-PEG-ZOL NPs for 30 and 90 min. Cells were washed, harvested and analyzed in FACS (Canto-II, BD), for the total amount of NP uptake by 10 000 cells. After similar treatment (as described above), adherent cells were washed and analyzed under confocal microscope (Carl Zeiss, Axiovert 135M), in a 8-well ibiTreat microscopy chamber (Ibidi, Martisried, Germany). The cell uptake route characterization was performed for 6-coumarin loaded PBCA-PEG NPs and PBCA-PEG-ZOL NPs, using various cell uptake route inhibitors, sodium azide (10 mM, energy-dependent endocytosis inhibition), wortmanin (10 μM, Macropinocytosis inhibition), phenyl arsine oxide (10 μM, clathrin type endocytosis inhibition) and genistein (200 μM, caveola type endocytosis inhibition). After treatment with the specific inhibitor, each well was tested for cell uptake of 6-coumarin loaded PBCA-PEG NPs and PBCA-PEG-ZOL NPs using FACS (Canto-II, BD).

2.5.2. NP Residence Time in Cells

BO2 cells were seeded on 6-well plates at the density of 1×10^5 cells per well and allowed to attach and grow. After 48 h, cells were incubated with 1 ml (100 μg/ml) 6-coumarin loaded PBCA-PEG NPs and PBCA-PEG-ZOL NPs for 90 min. Each well was washed with HBSS and incubated with 2 ml fresh HBSS. After 60, 120 or 240 min, cells were washed, harvested and analyzed in FACS for the total amount of NPs retained in 10 000 cells.

2.5.3. Cytotoxicity

The effect of DTX, DTX in combination with ZOL, DTX loaded PBCA NPs, PBCA-PEG NPs and PBCA-PEG-ZOL NPs on cell proliferation was determined using MTT based colorimetric assay.[14] Cells were plated onto flat-bottom 96-well plates at 5000 cells per well. After incubation for 24 h at 37 °C, medium was replaced with 200 μl medium containing varying concentrations of DTX, DTX-ZOL, DTX loaded PBCA-PEG NPs and PBCA-PEG-ZOL NPs, at 0.5, 2 and 8 nM/ml. After 48 and 72 h, medium was replaced with 100 μl medium containing MTT (500 μg/ml). After 1 h incubation, 100 μl SDS solution (20% w/v, water: DMF at 1:1 ratio, pH 4.7) was added, and further incubated for 24 h to dissolve the formazan crystals. The amount of MTT which is converted to formazan indicates the number of viable cells. The results were assessed in a 96-well format ELISA plate reader (Victor 1420, PerkinElmer), by measuring the absorbance at a wavelength of 570 nm. The IC_{50} was determined by nonlinear regression analysis using the equation for a sigmoid plot.[15]

2.5.4. Cell Cycle Analysis

The distribution of DNA in the cell replication state was studied by flow cytometry.[16,17] 1×10^5 cells per well were seeded on 6-well plate and allowed to attach and grow for 24 h. Cells were incubated with 2 ml media containing, 5 nM DTX, DTX loaded PBCA-PEG and PBCA-PEG-ZOL NPs. After 24 h, media was removed; cells were washed with PBS and harvested with 200 μl trypsin-EDTA. Incubation media, washing buffer and trypsin-EDTA treated cells were collected together and centrifuged at 1500 rpm for 5 min. The cell pellet was washed twice with PBS and centrifuged. Cells were re-suspended in 0.86 ml cold PBS, vortexed at slow speed and 2 ml absolute ethanol was added

drop wise to reach the final concentration of 70% v/v. After 15 min of incubation at 4 °C, cells were re-suspended in 250 µl staining PBS solution, composed of RNAse A (0.1 mg/ml), propidium iodide (10 µg/ml) and Triton X 100 (0.05%), and incubated at room temperature in the dark for 20 min. The cell cycle distribution was determined by analyzing 10 000 cells in FACS (Canto-II, BD) and recording signal from Texas red channel. Sections were made in the histogram of cell count vs. fluorescence/DNA content, to calculate the ratio of cells under Go/G1 (2n), S (2n+), G2/M phase (4n) and under apoptosis (2n–). Experiments were performed in triplicates.

2.5.5. Apoptosis using Annexin V-FITC

Induction of apoptosis was studied by flow cytometry using annexin V-FITC as a specific apoptotic marker.[16,17] 1×10^5 cells were seeded on 6-well plates and allowed to attach and grow for 24 h. Cells were incubated with 2 ml media containing (5 nM) DTX, DTX loaded PBCA-PEG and PBCA-PEG-ZOL NPs. After 48 h, cells were harvested and washed. 1×10^5 cells were suspended in 100 µl binding buffer and stained with PI (10 µl, 1 mg/ml) and Annexin V-FITC (5 µl), mixed well using vortex shaker and kept for binding. After 30 min, another 200 µl binding buffer was added and suspension was analyzed using FACS at Texas red and FITC channel (Canto-II, BD). The intensity plot of FITC vs. Texas red was sectioned into four quarters to differentiate stained and unstained cells. Based on the quarters, percentage of cells in early apoptosis (FITC positive and PI negative), late apoptosis (FITC and PI positive), and live cells (FITC and PI negative) were calculated.

2.5.6. IPP and Apppl Measurements

2.5.6.1. Cell Treatment and Sample Preparation for LC-MS: Sample treatment and preparation was performed as per earlier reported method.[18] MCF-7 and BO2 cells were seeded in 6-well plates at the density of 4×10^5 cells per well and incubated to allow cell attachment. After 24 h, cells were incubated with 2 ml media, containing 1 µg/ml ZOL solution and PBCA-PEG-ZOL NPs along with the control group (PBS) for 24 h. To extract analytes from cell line samples, cell culture plates were treated with ice cold acetonitrile (300 µl) followed by ice cold milliQ water (200 µl). The adherent cells were scrapped, mixed with pipette and centrifuged (13 000 × *g*, 3 min, 4 °C). The supernatant was transferred to another tube, and evaporated to complete dryness, using vacuum centrifugation and stored at –20 °C, until LC-MS analysis. Before analysis, the contents were dissolved in MilliQ water (150 µl) containing 0.25 mM NaF and Na_3VO_4 phosphatase inhibitors, and 1.0 µM AppCp as internal standard. The cell lysate precipitates were digested with 1 M NaOH at 60 °C for 2 h, and estimated for total protein content using modified Bradford procedure (Bio-Rad, Hercules, CA, USA), with bovine serum albumin as a standard protein on a plate reader (Wallac Victor2) at 595 nm. The final concentration of isopentenyl pyrophosphate (IPP) and triphosphoric acid 1-adenosin-5′-yl ester 3-(3-methylbut-3-enyl) ester (ApppI) was presented as nM per mg of protein.

2.5.6.2. Estimation of IPP and ApppI using LC-MS: All conditions have been previously described.[18,19] On-line HPLC-ESI MS measurements were carried out using an Agilent 6410 Triple Quad LC/MS for the analysis of IPP, ApppI and $AppCCl_2$ (standard). Instrument was equipped with an electrospray ionization source (EIS) and operated on negative ion mode. For the Agilent triple quadrupole instrument, optimized parameters were following: drying gas temperature was 300 °C, gas flow at 8 ml/min, nebulizer gas pressure operated at 40 psi and capillary voltage was –4500 V. Negative full scan mass spectra were performed in the mass range of m/z 60–650 at above mentioned conditions. Parent ion abundance with highest intensity was indentified using fragmentor voltages of 120 V for IPP, 140 V for ApppI, and internal standard (ISTD) AppCp. Individual product ion (MS2) spectra were recorded using collision induced dissociation (CID), in the collision cell with nitrogen gas. The most intense product ion signal was achieved when offset voltages were 15, 27 and 30 eV for detection of IPP, ApppI and internal standard (AppCp) respectively. Following transitions were optimized for multiple reactions monitoring (MRM): m/z 245 → 79 for IPP, m/z 574 → 227 for ApppI and m/z 504 → 157 for internal standard (AppCp). Agilent Mass Hunter Workstation software was used for data acquisition.

2.5.6.3. Quantification of the Total Amounts of IPP/DMAPP and ApppI/ApppD: The analysis method was validated using IPP and ApppI standards. The limit of quantification (LOQ) was calculated as the lowest estimation with the percent relative standard deviation (RSD%) value lower than 20% and the signal-to-noise ratio remained greater than 10:1. All calibration samples were prepared fresh on each day of analysis. The calibration area was selected in range from 0.001 µM to 90.0 µM for IPP and from 0.001 µM to 30.0 µM for ApppI. The calibration curve was obtained in triplicate measurements. Ratio of peak area of analytes and internal standard were plotted against the concentration of the standards.

2.6. Pharmacokinetics by Radio Label Technique

The formulations were radio labeled using technetium (^{99m}Tc) by earlier reported methods.[20,21] Technetium in sodium pertechnetate was reduced in the acidic condition in the presence of stannous chloride and then allowed to react with NPs which forms NPs tagged with technetium.

2.6.1. Labeling Efficiency

The radiolabeling efficiency of the formulations were estimated using thin layer chromatography (TLC). Silica gel-coated fiberglass sheets (Gelman Sciences, MI) were used as a stationary phase, while solvent system consisting of acetone and pyridine:acetic acid:water (3:5:1.5 v/v) was used as a mobile phase.[22] The unlabeled technetium has R_f value of around 1, while labeled NPs were retained at R_f value near to zero. So, the ratio of radioactivity in the top 1/3 to lower 2/3 of the TLC was considered as the percentage labeling efficiency.

2.6.2. Biodistribution Studies

All animal experiments were approved by the Committee for the Purpose of Control and Supervision of Experiments on

Animals (CPCSEA), Ministry of Social Justice and Empowerment, Government of India, New Delhi, India. Swiss mice (aged 6 to 8 weeks), weighing between 20 to 25 g, with tumor (1 to 1.5 cm, Ehrlich ascites tumor) in bone were selected for the study. Each formulation and time point was tested in triplicate. Radio labeled formulations (100 µl) was injected into the tail vein of the mice. Mice were sacrificed at different time intervals by cervical dislocation, and the tissue/organs (blood, liver, tumor, brain, heart, lung, kidney, stomach, intestine, muscle, bone bearing tumor and bone without tumor) were isolated. The collected tissue/organs were estimated for the presence of radioactivity, using gamma scintillation counter, and calculated as a fraction of total dose administered using the below equation:[23]

$$\%\ \text{Radioactivity per g of tissue} = \frac{\text{Counts in sample} \times 100}{\text{Wt of sample} \times \text{Total counts injected}}$$

2.7. Statistical Analysis

The results are reported as mean ± SD. The difference between the groups was tested using two way analysis of variance (ANOVA), followed by Bonferroni posttests using Graph Pad Prism 5.0, and the differences were considered to be statistically significant when $p < 0.05$.

3. Results and Discussion

3.1. Physiochemical Characterization of PBCA-PEG-ZOL NPs

In an attempt to formulate pegylated PBCA NPs for bone targeting, DTX loaded pegylated PBCA NPs were developed by modified anionic polymerization technique. Preparation of PBCA-PEG-ZOL was carried out by first preparing ZOL-PEG-amine conjugate using CDI as a linker and activator. The FTIR spectra of the PBCA (Figure S1, Supporting Information) show C–H (str) at 2957 cm^{-1} and C–H (def) at 1461 cm^{-1}. The characteristic C≡N (str) of the polymer was observed at 2200 cm^{-1}. The presence of characteristic peaks of PEG and ZOL with PBCA demonstrated successful conjugate formation. NMR spectra of PBCA-PEG-ZOL NPs (Figure S2, Supporting Information) showed a strong peak at 3.5 ppm demonstrating the presence of PEG ($-CH_2-O-CH_2-$). Characteristic peaks from zoledronate (3.35 ppm) also confirm conjugation of PBCA-PEG-ZOL.

In the second stage, this prepared conjugate was added in a reaction media of PBCA-PEG NP, where free amine group of ZOL-PEG-amine work as an initiator template for polymerization reaction, which later forms PBCA-PEG-ZOL NPs. A successful nanoparticulate system ideally has a high entrapment efficiency to reduce the quantity of the carrier required for administration. DTX was efficiently entrapped in pegylated PBCA-NPs, 77.38 ± 3.20% with a loading capacity of 3.69 ± 0.15% as estimated by HPLC. ZOL conjugated NPs showed 75.94 ± 3.82% entrapment efficiency, which is not significantly different when compared with un-conjugated NPs. Particle size analysis revealed that the PBCA-NPs had a unimodal size distribution with a mean hydrodynamic diameter of 118 ± 6.35 nm (**Figure 1**a) having a zeta potential of –17.64 ± 2.21 mV (Figure 1b and **Table 1**). Surface modification of PBCA-NPs with PEG showed minor changes on its physical characteristics. A decrease in size (from 118 ± 6.35 to 81 ± 5.63 nm) and zeta potential (from –17.64 ± 2.21 mV to –8.26 ± 1.26 mV) was observed. Surface modification of pegylated PBCA-NPs with ZOL had particle size of 82 ± 6.35 nm which is not different from that of PBCA-PEG NPs, whereas, zeta potential of ZOL conjugated formulation showed a difference from –8.26 ± 1.26 mV to –23.51 ± 3.37 mV. TEM images (Figure 1c) showed discrete spherical shaped PBCA-PEG-ZOL NPs of particle size less than 100 nm. As shown in Figure 1d, DTX loaded PBCA-PEG NPs exhibited a biphasic drug release pattern, that was characterized by a first initial rapid release in which 15.86 ± 0.92% DTX was released in 8 h, followed by a slower continuous release phase in which 74.48 ± 1.42% of DTX was released in 5 days. Similar release pattern was also observed for release of DTX from PBCA-PEG-ZOL NPs. No significant difference ($p > 0.05$) in percentage drug release of PBCA-PEG NPs and PBCA-PEG-ZOL NPs was observed at any time point. Schematic representation of the expected surface modifications of the NPs with zoledronic acid is shown in **Scheme 1**.

3.2. In Vitro Bone Binding Assay, Quantitative Cell Uptake, Confocal Microscopy and NPs Uptake Route Characterization

In vitro bone binding affinity showed that both ZOL solution and PBCA-PEG-ZOL NPs had strong affinity with human simulated bone–hydroxyapatite powder. After 1 h, 42.2 ± 3.2%

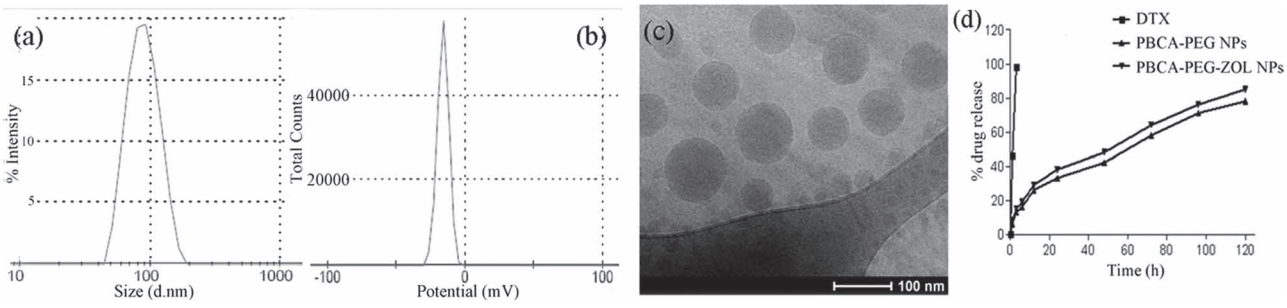

Figure 1. Characterization of PBCA-PEG-ZOL NPs. a) Particle size distribution, b) zeta potential, c) cryoTEM image, and d) % in vitro drug release profile (some error bars are too small to be shown).

Table 1. Physicochemical characterization of PBCA NPs and PEGylated PBCA NPs.

Formulation	Particle size [nm]	Zeta potential [mV]	% Drug entrapment	% Drug loading
PBCA NPs	118 ± 6.35	–17.64 ± 2.21	43.07 ± 2.43	2.05 ± 0.11
PBCA-PEG NPs	81 ± 5.63	–8.26 ± 1.26	77.38 ± 3.20	3.69 ± 0.15
PBCA-PEG-ZOL NPs	82 ± 6.35	–23.51 ± 3.37	75.94 ± 3.82	3.62 ± 0.23

ZOL was found in bone powder while PBCA-PEG-ZOL NPs showed 31.7 ± 4.2% localization (**Figure 2**). With an increase in the incubation time, binding affinity of ZOL as well as NPs increased to 94.1 ± 7.2% and 83.5 ± 7.4%, respectively. The affinity of ZOL as well as ZOL conjugated NPs to the human simulated bone–hydroxyapatite powder was found to be significantly higher at 4 h ($p < 0.05$) and 12 h ($p < 0.01$), compared to 1h of incubation. In vitro bone binding results confirmed that ZOL has strong binding affinity with human simulated bone–hydroxyapatite powder, even when used as a surface ligand conjugated to NPs. The intracellular fate of the macromolecular carriers is strongly affected by the route of entry. Many endocytic pathways for macromolecules have been identified: clathrin-mediated endocytosis, caveolae-mediated endocytosis, macropinocytosis, and clathrin and caveolae-independent endocytosis.[24–27] In order to identify the uptake mechanisms involved in the cellular entry of NPs, various cell uptake route inhibitors were used to determine the intracellular route for NPs trafficking in BO2 cell line.

Physicochemical properties like molecular weight, particle size, shape, surface charge and composition plays a key role in the cellular uptake of polymeric NPs.[28] It is crucial to understand that the alteration of each specific property may impact differently on the uptake behavior depending on the type of cell and the structure of the NP itself. Uptake pathway regulation can be fulfilled considerably by adjusting the particle size, because the internalized NP tends to be trapped in intracellular vesicles, and each endocytic pathway generates a distinct size range of endocytic vesicles.[29] Some relevant studies on the particle size dependency described that smaller particles (<100 nm) with a uniform size distribution showed a higher degree of uptake by tissue.[30] However, some chitosan-based NPs did not necessarily display such correlation with decreasing particle size,[31,32] suggesting that the size of NPs may not be the only dominant factor to influence the uptake. Surface properties of NPs can affect the internalization process. For example, NPs with hydrophobic surface were taken up to a greater extent via endocytosis or phagocytosis, than the similar sized particles with hydrophilic surface.[33,34] Surface charge also exerted influence on the cellular uptake. NPs bind strongly to the cell membrane and display a higher cellular uptake when the surface charge is higher, where electrostatic interactions between the anionic membrane and cationic NPs facilitated the uptake.[35] Another study using PLGA discussed that the change of surface charge in the acidic endolysosomal environment induced the release of NPs to the cytoplasm.[36] Thus, the formulation of NPs with different surface properties can influence their cellular uptake and intracellular distribution. Overall, research of the uptake behavior by changing physicochemical properties is to be pursued for each type of nanocarriers.

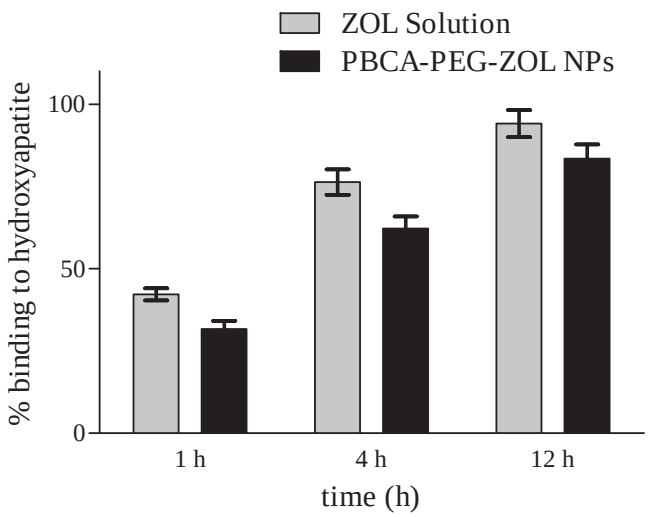

Figure 2. In vitro bone binding affinity to ZOL solution and PBCA-PEG-ZOL NPs in human simulated bone–hydroxyapatite powder.

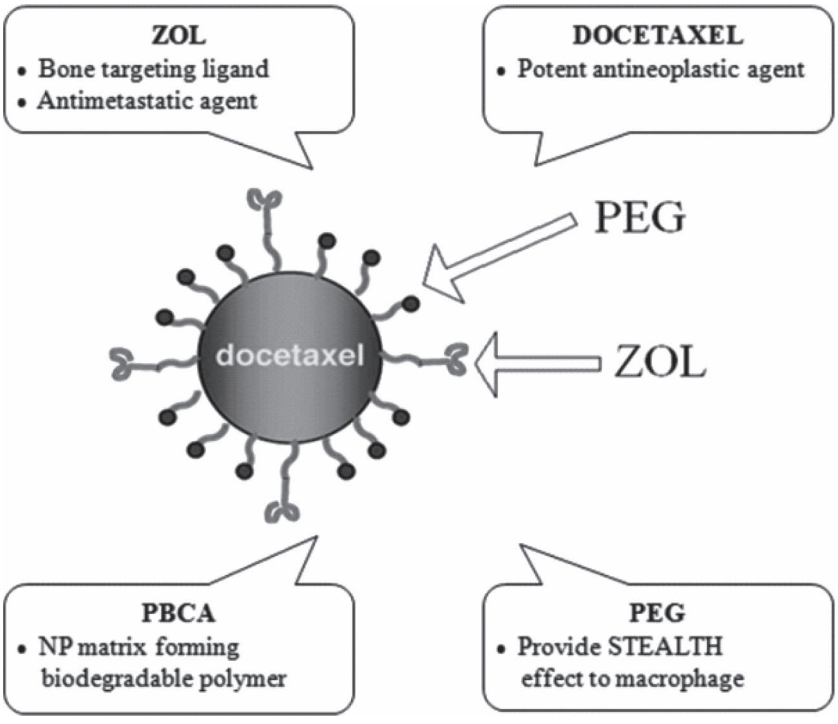

Scheme 1. Schematic representation of the expected surface modifications of the nanoparticles with zoledronic acid.

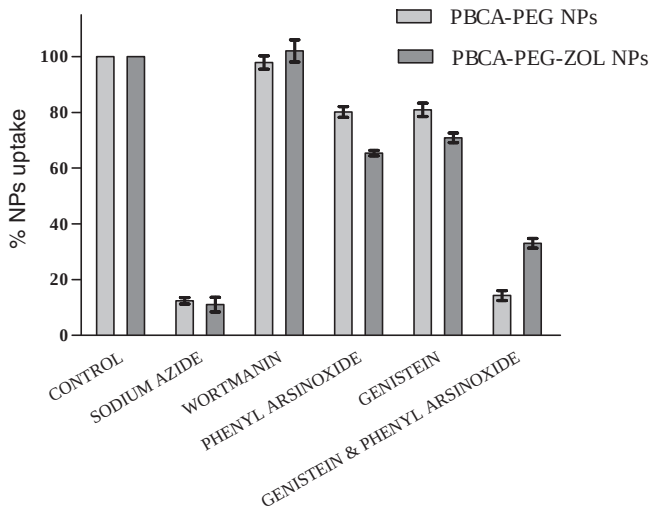

Figure 3. Characterization of route for NPs uptake by various endocytosis inhibitors on BO2 cell line using 6-coumarin loaded PBCA-PEG NPs and PBCA-PEG-ZOL NPs. Data presented as mean ± SEM, n = 3.

In this study, treatment with sodium azide reduced NPs uptake up to 88% indicating the internalization mechanism was an energy dependent process for both PBCA-PEG NPs and PBCA-PEG-ZOL NPs (**Figure 3**). Increase in concentration of both NPs from 50 to 200 μg/ml shows reduction in fraction uptake. The trend demonstrated that the process followed saturable kinetic and eliminate the possibility of macropinocytosis uptake, which follows the linear uptake kinetic.[37] The size of the NPs are approximately 100 nm, which is very low in comparison to the threshold required for phagocytosis activation, which requires the particles to be bigger than 1 μm.[38] Treatment of BO2 cells with wortmanin (micropinocytosis inhibitor), showed no significant change ($p > 0.05$) in the uptake of PBCA-PEG NPs and PBCA-PEG-ZOL NPs, which confirms the presence of non-micropinocytosis pathway (Figure 3). After treatment with phenyl arsinoxide (clathrin mediated endocytosis inhibitor), PBCA-PEG NPs demonstrated 80.16% uptake, while PBCA-PEG-ZOL NPs displayed 65.38% uptake. While in case of genistein treatment (caveolae-mediated endocytosis inhibitor), PBCA-PEG NPs demonstrated 80.94% uptake while PBCA-PEG-ZOL NPs showed 70.87% uptake. However, after the treatment with both, genistein and phenyl arsinoxide, the PBCA-PEG NPs uptake was reduced dramatically to 14.28%, suggesting the uptake was based on both clathrin, and caveolae mediated endocytosis (Figure 3). Whereas, PBCA-PEG-ZOL NPs uptake was not completely blocked even by using both inhibitors simultaneously, this confers that PBCA-PEG-ZOL NPs uptake was not entirely based upon clathrin and caveolae mediated endocytosis.

The cellular uptake of PBCA-PEG NPs and PBCA-PEG-ZOL NPs were evaluated in MCF-7 and BO2 cell lines. In case of MCF-7 cells, uptake of PBCA-PEG-ZOL NPs after 30 min was found to be 82.54%, which is 1.62 times higher than PBCA-PEG NPs (**Figure 4**a). Internalization of PBCA-PEG-ZOL NPs reached 100% within 120 min, while only 63.92% PBCA-PEG NPs were internalized at the same time point. Similar results were found when cellular uptake was studied using BO2 cell line (Figure 4b). Across all time points, the uptake of PBCA-PEG-ZOL NPs was found to be more than 1.4 times higher than PBCA-PEG NPs.

Understanding the intracellular trafficking through the endolysosomal pathway, and the fate of NPs with respect to their uptake mechanisms are crucial in understanding the intracellular fate of the NPs. Unfortunately, determination of the exact intracellular trafficking pathway of NPs is difficult due to the fast dynamics of maturation and un-noticeable morphological changes between endosomal and lysosomal compartments. To track the uptake of PBCA-PEG NPs and PBCA-PEG-ZOL NPs, the lysosomes of BO2 cells were stained with the LysoTracker Red probe after the treatment with 6-coumarin loaded PBCA-PEG NPs and PBCA-PEG-ZOL NPs. The cell nucleus was labeled with Hoechst 33342. The intracellular localization of the PBCA-PEG NPs and PBCA-PEG-ZOL NPs were traced after 120 min incubation (**Figure 5**). The co-localization of the green fluorescence of 6-coumarin loaded NPs with the red fluorescence from lysosomes produced a yellow fluorescence, as evident from the merged images. Images showed few co-localization of PBCA-PEG NPs with the lysosomes, but the co-localization was negligible in PBCA-PEG-ZOL NPs treated cells. These results

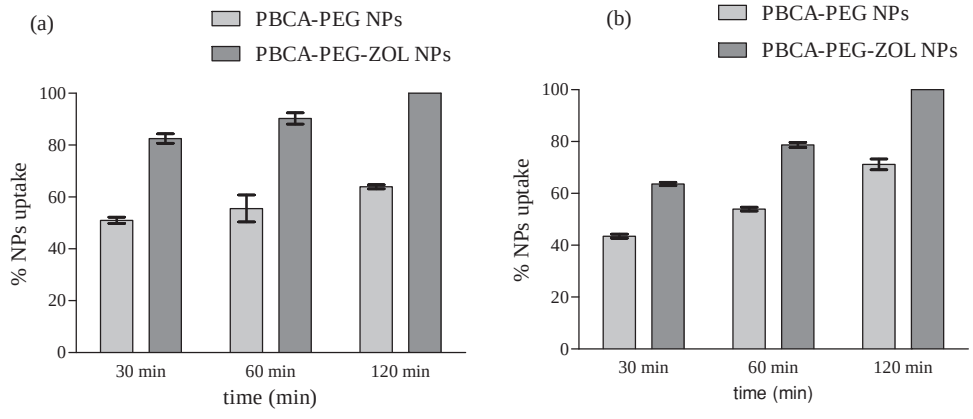

Figure 4. Retention time of PBCA-PEG NPs and PBCA-PEG-ZOL NPs in intracellular compartment in MCF-7 and BO2 cell line after incubation for 30, 60 and 120 min using FACS as estimation technique. Data presented as mean ± SEM, n = 3.

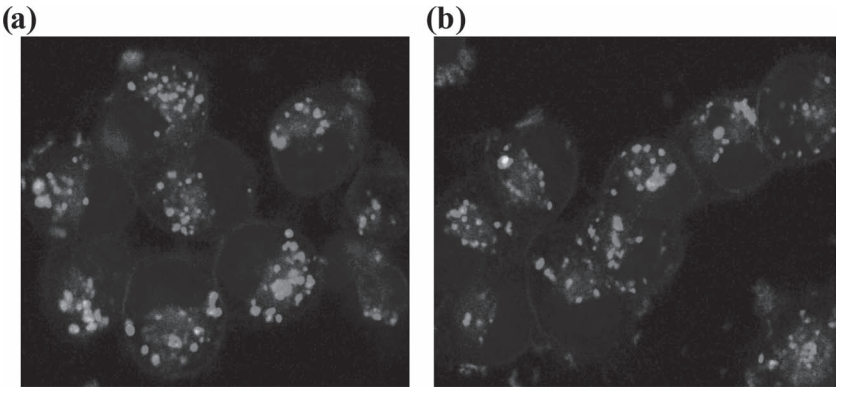

Figure 5. Microscopic evaluation of PBCA-PEG-ZOL NPs uptake performed using confocal microscope in BO2 cell line. 6-coumarin loaded NPs were added to the BO2 cells, followed by staining with LysoTracker Red, and Hoechst 33342 for lysosome and nucleus, respectively. Panels (a,b) show overlapping images for PBCA-PEG-ZOL NPs. Yellow color indicates NPs in lysosomal compartment.

were in relevance to the route characterization results in which PBCA-PEG-ZOL NPs were less co-localized. These demonstrate that NPs were endocytosed by both the clathrin and caveolae mediated endocytosis mechanism, where the caveolae pathway followed a non-lysosomal route. PBCA-PEG NPs were carried to the lysosomes through early endosomes, which displayed few co-localization of NPs and lysosomes. However, PBCA-PEG-ZOL NP showed negligible co-localization, and the uptake was not dependent on clathrin mediated endocytosis.

3.4. NP Residence Time in Cells

Residence time of NPs in cells was studied to correlate therapeutic efficacy of un-conjugated PBCA NPs and ZOL conjugated PBCA NPs. Study of the residence time of NPs in cells is important in determining the intracellular fate (or successful delivery system or therapeutic success) of the drug delivery system. Residence of NPs inside the cell depends upon the route of intracellular uptake of NPs. When intracellular drug delivery is desired specially in case of cytotoxic drug, longer duration of residence is desirable to allow complete release of the entrapped drug into the cytoplasm.[16] In this study, percentage NPs retention with time was carried out for un-conjugated and ZOL conjugated PBCA-PEG NPs. Results demonstrated that after 60 min, ZOL conjugated NPs showed two times longer residence time than un-conjugated ones (**Figure 6**). After 240 min this ratio increases to three times. As time increases, the residence time of NPs decreases for both formulations. This is possibly due to the fact that, the concentration of NPs in the extracellular domain of the cell drop, and the equilibrium gets disturbed, when NPs were removed from the external media, resulting in sharp reduction of the intracellular NPs levels.[39]

3.5. Cell Cytotoxicity

The therapeutic potentialities of different conjugated and un-conjugated nanoparticulate formulations (DTX loaded PBCA-PEG NPs and PBCA-PEG-ZOL NPs) were compared with DTX solution and DTX-ZOL mixture in a dose dependent and time dependent manner, in MCF-7 and BO2 cell lines using MTT based cell proliferation assay.[40] From results, it was observed that no cytotoxicity was observed in case of cells treated with same concentration of blank PBCA-PEG NPs as that of PBCA-PEG-ZOL NPs. PBCA-PEG-ZOL NPs exhibited significantly very lower IC_{50} values as compared to DTX, DTX-ZOL mixture and PBCA-PEG NPs across all time points in both cell lines. The IC_{50} values of PBCA-PEG-ZOL NPs were found to be approximately 10 times lower than that of DTX and DTX-ZOL mixture after 72 h of incubation in both cell lines.

The IC_{50} value for MCF-7 cells treated with PBCA-PEG-ZOL NPs was found to be 2.49 nM at 48 h, which was 2.6, 2.7 and 1.4 times less than DTX, DTX-ZOL and PBCA-PEG NPs respectively (**Figure 7**). Exposure for 72 h further lowered the IC_{50} value by 1/5 of its value to 0.46, which was more than 11 times less, in comparison with DTX solution. Incubation of BO2 cells with PBCA-PEG-ZOL NPs also resulted in enhanced cytotoxic effects, when compared with DTX and un-conjugated NPs formulations. The IC_{50} value for BO2 cells treated with PBCA-PEG-ZOL NPs was found to be 0.36 nM after 72 h, which was 9.4, 9.0 and 7.2 times less than DTX, DTX-ZOL and PBCA-PEG NPs. There was a significant decrease to about 5 and 6 times in IC_{50} values for MCF-7 and BO2 cell lines, respectively, when compared with un-conjugated formulations at two different time points. This significant difference in IC_{50} values of un-conjugated NPs and ZOL conjugated NPs, at 48 and 72 h of exposure in MCF-7 and BO2 cells, clearly indicates that the higher cytotoxic effect of PBCA-PEG-ZOL NPs in cell lines is mediated by surface functionalization of NPs with ZOL. PBCA-PEG-ZOL NPs were found to be more toxic to BO2 cells, when

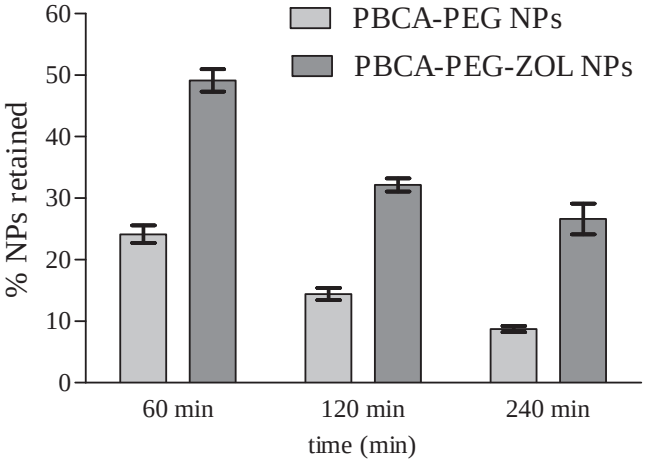

Figure 6. Residence time of PBCA-PEG NPs and PBCA-PEG-ZOL NPs in BO2 cell line, following incubation for 60, 120 and 240 min, using FACS as estimation technique. Data presented as mean ± SEM, n = 3.

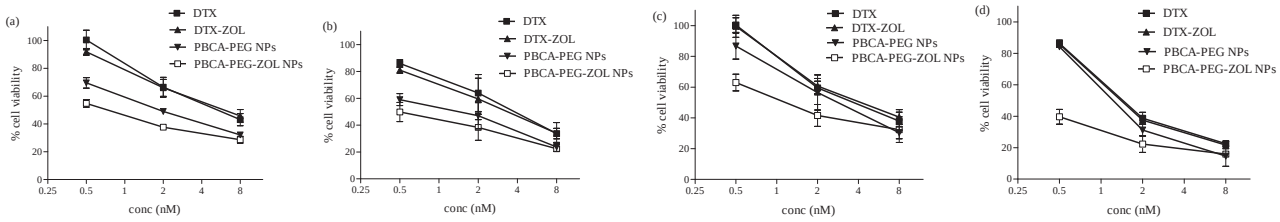

Figure 7. Cytotoxicity study of DTX solution, ZOL-DTX solution, DTX loaded PBCA-PEG NPs and PBCA-PEG-ZOL NPs in MCF-7 (a,b), and BO2 cell line (c,d), after 48 h (a,c), and 72 h (b,d), using MTT assay. Data presented as mean ± SEM, n = 3.

compared with MCF-7 cells. It was demonstrated by Panyam et al. that NPs rapidly escape the endolysosomes and enter the cytoplasm.[36] The fractions of NPs that escape the endosomes seem to remain in the cytoplasm and release the encapsulated drug in a sustained manner.[14]

Thus, it can be speculated that the anti-tumor mechanism of PBCA-PEG-ZOL NPs is through their binding and getting internalized into tumor cells with a subsequent intracellular release of DTX after PBCA degradation.[41] Hence, we can conclude that drug loaded NPs have enhanced therapeutic efficacy when compared to drug solution. However, in this study, we found that conjugation of ligand to NPs further enhances its therapeutic effectiveness to a higher level, in comparison to drug solution, drug-ligand mixture and un-conjugated NPs. These findings were in accordance to previous work.[27,42]

3.6. Cell Cycle Analysis

Analysis of a cell population in each replication state can be achieved by fluorescence labeling of the nuclei with PI staining, and then estimating DNA content by FACS analysis.[43] Cell cycle analysis was performed in BO2 cell line after treatment with DTX, DTX loaded PBCA-PEG and PBCA-PEG-ZOL NPs. **Figure 8** represents cell cycle distribution of control group having 62.35 ± 2.64% cells in G0/G1 phase, 12.69 ± 1.02% in S phase, 22.89 ± 1.23% cells in G2/M, and only 2.07 ± 0.22% cells in Sub G0/G1 phase. After treatment with DTX, the cell cycle arrest can be seen, and the majority of cells (60.74 ± 2.29%) were arrested at G2/M check point, with only 6.31 ± 0.53% cells at Sub G0/G1 phase. Treatment with PBCA-PEG NPs showed similar blockage at G2/M check point, as compared to DTX treatment, but almost 245% increase (15.49 ± 0.86%) at Sub G0/G1 phase was observed, which represents increased apoptosis. After treatment with PBCA-PEG-ZOL NPs, blockage at G2/M check point does not change significantly, as DTX and PBCA-PEG NPs treatment led to significant increase in amount of apoptotic cells at Sub G0/G1 phase, showing higher amount of cells undergoing apoptotic cell death (2.5 and 6.2 times, as compared to PBCA-PEG NPs and DTX, respectively). This signifies the effectiveness of PBCA-PEG-ZOL NPs

	G0/G1	S	G2/M	Sub G0/G1
CONTROL	62.35 ± 2.64%	12.69 ± 1.02%	22.89 ± 1.23%	2.07 ± 0.22%
DTX	21.72 ± 1.3%	11.23 ± 0.81%	60.74 ± 2.29%	6.31 ± 0.53%
PBCA-PEG20 NP	23.32 ± 1.14%	9.81 ± 0.94%	51.38 ± 2.46%	15.49 ± 0.86%
PBCA-PEG-ZOL NP	18.07 ± 1.16%	6.39 ± 0.69%	36.19 ± 1.27%	39.35 ± 2.09%

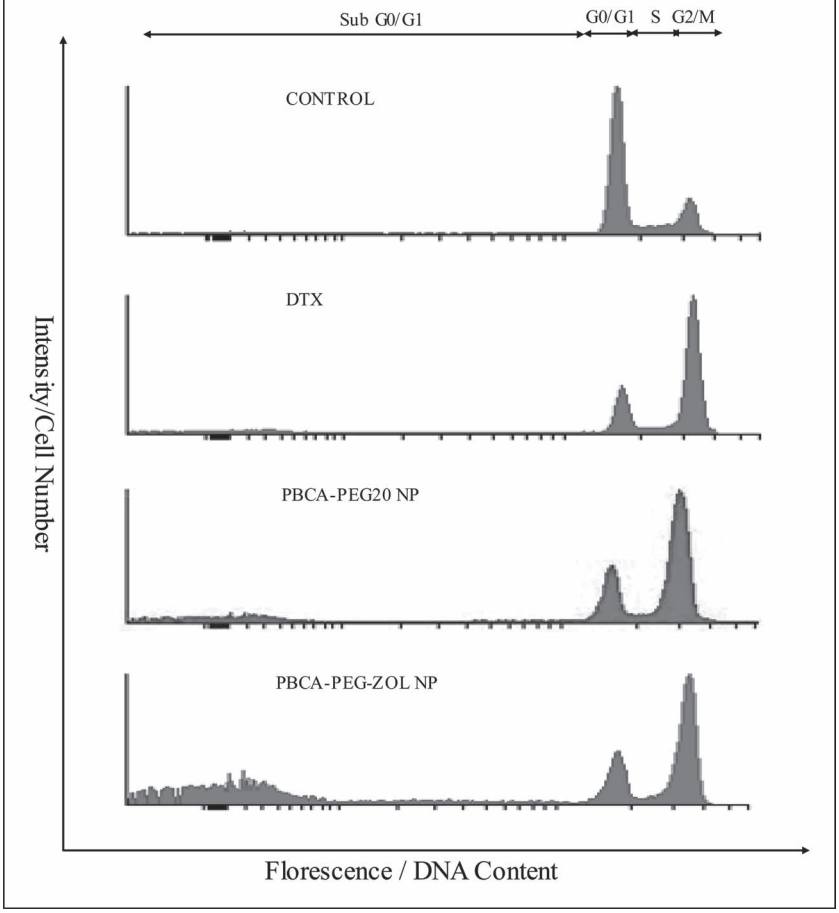

Figure 8. Cell cycle analysis in BO2 cell line after treatment of a) control (PBS) and b) DTX solution. DTX loaded c) PBCA-PEG NPs and d) PBCA-PEG-ZOL NPs, by PI staining, using FACS technique. Data presented as mean ± SEM, n = 3.

as an effective carrier for DTX, among tested formulations. It can be believed that in case of NP mediated targeted therapy: more drug is available at the site of action (following sustained drug release) for a longer period of time, than the drug in solution, resulting in greater efficiency of the NP in arresting cell growth. ZOL could have facilitated the intracellular delivery of DTX loaded NP, thus better allowing DTX and ZOL induced cytotoxicity, resulting in higher inhibition of cell proliferation.

3.7. Apoptosis using Annexin V-FITC

Cells undergoing apoptosis show characteristic morphological and biochemical features. The characteristics include chromatin aggregation, nuclear and cytoplasmic condensation, while necrosis displays a direct injury to the cell. Determination of cell death mechanism is important to compare effectiveness of NP formulations. Apoptosis study of the prepared NPs was conducted using Annexin V staining procedure in MCF-7 and BO2 cell lines. This assay takes advantage of the fact that phosphatidylserine (PS) is translocated from the inner (cytoplasmic) leaflet of the plasma membrane to the cell surface, soon after the induction of apoptosis. Annexin V protein has a strong, specific affinity for PS which can be used as a probe for estimation.[44] In MCF-7 cells, control treatment group showed negligible presence of apoptosis and necrotic cells (less than 4%) (**Figure 9**a). The percentage of late apoptotic cells was higher in case of cells treated with DTX loaded PBCA-PEG-ZOL NPs (32.58%), than DTX loaded PBCA-PEG NPs (23.03%) or DTX (14.72%), which is almost 1.4 and 2.2 times. While DTX had very few cells in pro-apoptotic phase (2.14%), DTX loaded PBCA-PEG NPs showed almost 2 times pro-apoptotic cells (3.97%), whereas DTX loaded PBCA-PEG-ZOL NPs showed 7.79% cells, within pro-apoptotic phase. Thus, DTX loaded PBCA-PEG-ZOL NPs were able to cause a significant increase in programmed cell death, in comparison with the cells treated with DTX and DTX loaded PBCA-PEG NPs.

In apoptosis study with BO2 cell line, similar results were obtained with increased pro-apoptotic (from 0.43% in control cells to 13.61% in PBCA-PEG-ZOL NPs treated cells) (Figure 9b). We found major presence of late apoptotic and early apoptotic phase, when treated with DTX, DTX loaded PBCA-PEG and PBCA-PEG-ZOL NPs. Control treatment again showed less than 4% of total cell death. In BO2 cells, DTX loaded PBCA-PEG-ZOL NPs showed 36.39% cells with late apoptosis, which was higher, as compared to DTX solution (7.46%) and DTX loaded PBCA-PEG NPs (20.9%). The distributions of early apoptotic cells were 6.07%, 12.47% and 13.61% for DTX solution and DTX loaded PBCA-PEG NPs and PBCA-PEG-ZOL NPs, respectively. After internalization, NPs might activate apoptotic signals at much reduced dose by dipping threshold required for activation. Targeted delivery had shown enhanced apoptotic activity by more RME which made more drugs available for action. Sustained cytoplasmic delivery of the DTX from NPs, coupled with ZOL, resulted in enhanced therapeutic potency of the NPs, by apoptosis, as compared to the un-conjugated NPs, thus supporting the hypothesis that ZOL modified NPs can serve as effective delivery vehicles to bone metastasis and cancer.

3.8. IPP and Appp I Measurements

ZOL appears to inhibit farnesyl pyrophosphate (FPP) synthase in the mevalonate pathway without metabolizing itself.[45,46] Inhibition of FPP synthase prevents the post-translational modification of important signaling proteins through addition

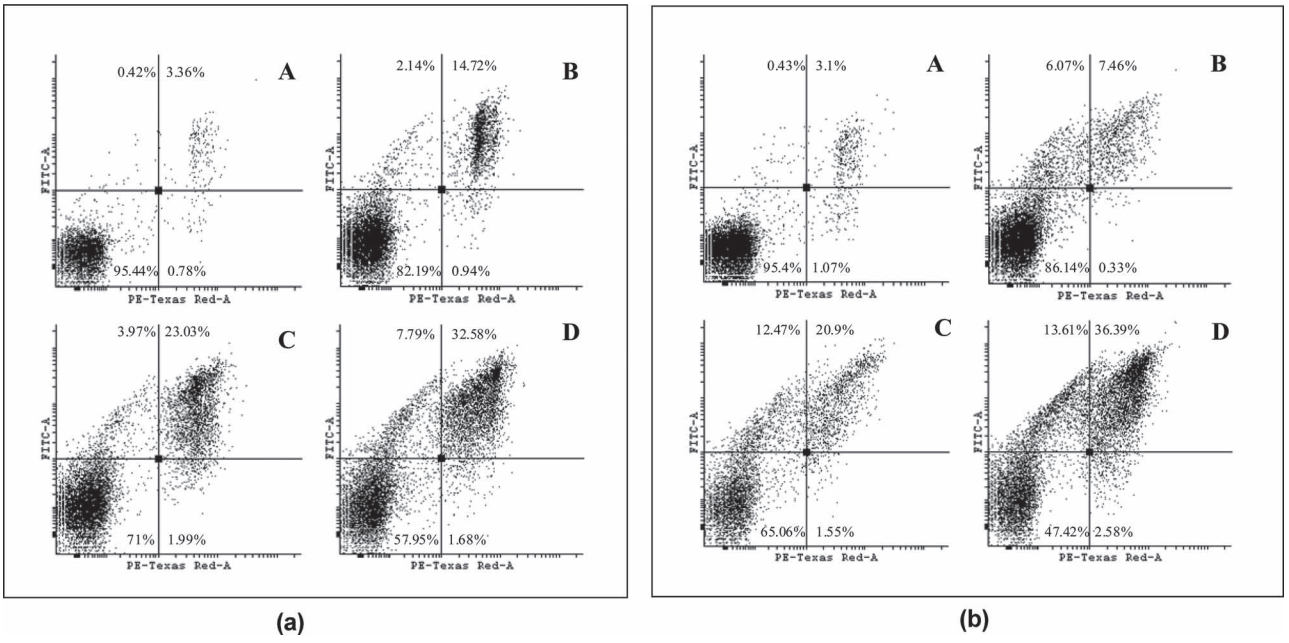

Figure 9. Apoptosis estimation in a) MCF-7 and b) BO2 cell lines after treatment of control (PBS), A; DTX solution, B; DTX loaded PBCA-PEG NPs, C; PBCA-PEG-ZOL NPs, D, by Annexin V-FITC and PI staining using FACS technique. Dead cells FITC (–), PI (+); early apoptotis FITC (+), PI (–); live FITC (–), PI (–); late apoptosis FITC (+), PI (+).

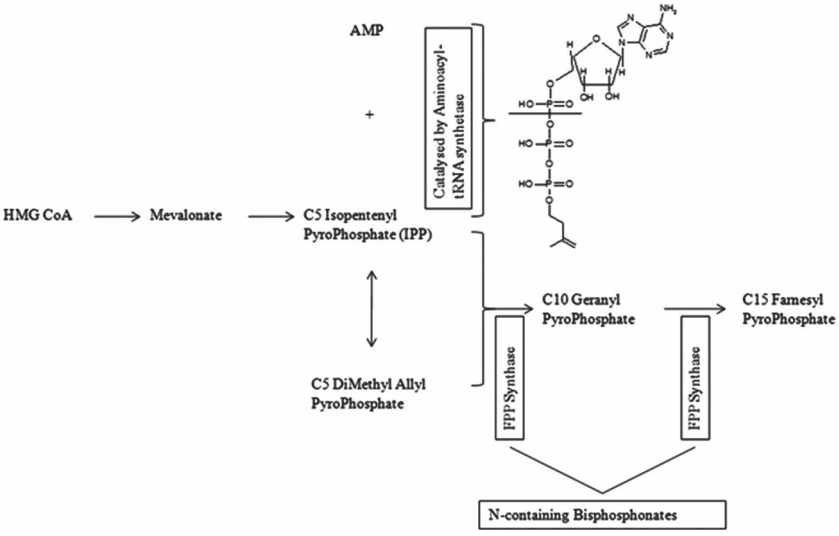

Figure 10. Mechanism of action for ZOL which induces formation of a new type of ATP analog, ApppI. ApppI formation is due to the inhibition of FPP synthase in the mevalonate pathway and consequent accumulation of the intracellular IPP is catalyzed by the amino acyl-tRNA-synthetases.

of isoprenoid lipids. Loss of prenylated proteins results in loss of cellular function, leading to indirect apoptotic cell death.[47] Monkkonen et al. revealed a new mechanism of action for ZOL which induces formation of a new type of ATP analog, ApppI (triphosphoric acid 1-adenosin-5′-yl ester 3-(3- methyl- but-3-enyl) ester), without a bisphosphonate structure.[47] ApppI is formed due to the inhibition of FPP synthase in the mevalonate pathway and consequent accumulation of the intracellular isopentenyl pyrophosphate (IPP), which is catalyzed by the amino acyl-tRNA-synthetases (**Figure 10**). ApppI induces direct apoptosis through the blockade of the mitochondrial ADP/ATP translocase.[47]

Amount of IPP and ApppI were estimated in BO2 and MCF-7 cell lines after treatment with ZOL and PBCA-PEG-ZOL NPs. Fraction of protein was separated by extraction using acetonitrile:water after cell lysis and estimated using HPLC-ESI-MASS instrument. Results showed that treatment with ZOL solution in MCF-7 cell line found to increase IPP production, more than 19 times than the control group treated with PBS (**Figure 11**a). Treatment with PBCA-PEG-ZOL NPs showed 7 times increase in IPP production in comparison to ZOL solution treatment, and 138 times higher than the control group. ApppI level in MCF-7 cell line after the treatment with PBCA-PEG-ZOL NPs, was found to be 5.3 times higher than the treatment with ZOL solution (Figure 11b). In case of BO2 cell line, IPP production after the treatment with PBCA-PEG-ZOL NPs was 5.35 times higher than ZOL solution, and IPP level in the control group was below the detection level (Figure 11c). However, no ApppI production in BO2 cell line after treatment with PBCA-PEG-ZOL NPs and ZOL solution was found, which was as per our previous experience, as BO2 cell line does not produce detectable levels of ApppI. Treatment with DTX did not result in the production of IPP or ApppI at any concentration. Results confer that ZOL conjugated to PBCA-PEG NPs can significantly enhance the action of ZOL in both the cell lines.

3.9. Biodistribution Studies

The biodistribution was assessed at three different time point, 1, 4 and 24 h after intravenous administration of DTX, DTX loaded PBCA NPs, PBCA-PEG NPs and PBCA-PEG-ZOL NPs. The comparative biodistribution of free DTX and its formulations are shown in **Figure 12**. It was observed that free DTX achieved maximum concentration within 1 h in all organs and was quickly eliminated from the body, than any of its nanoparticulate formulation. When DTX was administered as free drug, rapid elimination from the circulation was observed, with more than 1/5 DTX eliminated from the blood compartment.[48,49] In case of PEGylated PBCA NPs, delayed blood clearance was observed at 24 h, with more than 5 times of formulations left in the blood. This suggests the design of NP constructs with highly flexible PEG chains on its surface would prevent opsonisation indicating long circulation capability, as reported by other authors.[50,51] As shown in Figure 12, free DTX was mainly distributed to the liver (3.3 ± 0.5%/g), heart (2.3 ± 0.2%/g), kidney (2.3 ± 0.3%/g) and brain (2.1 ± 0.2%/g), after 1 h, whereas PBCA NPs and PBCA-PEG

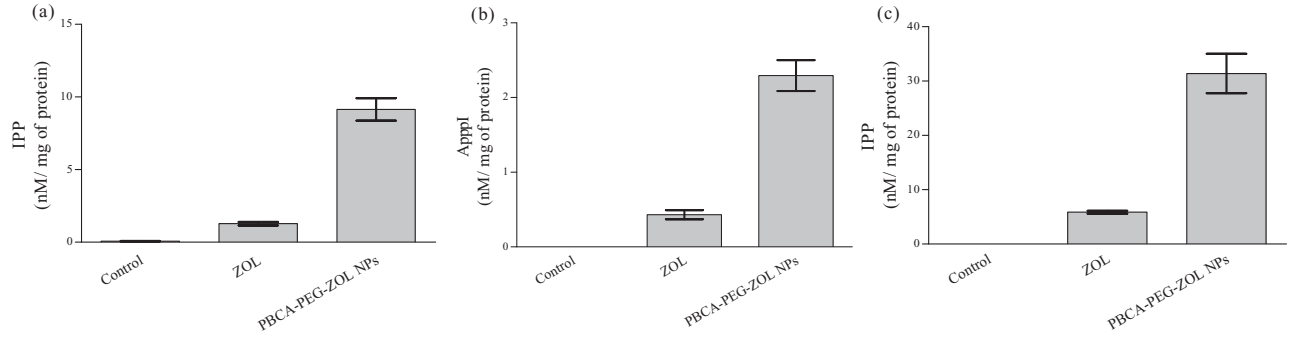

Figure 11. IPP and ApppI retention after treatment with ZOL solution and PBCA-PEG-ZOL NPs along with control (PBS). a) IPP in MCF-7 cell line, b) ApppI in MCF-7 cell line, and c) IPP in BO2 cell line. Data presented as mean ± SEM, n = 3.

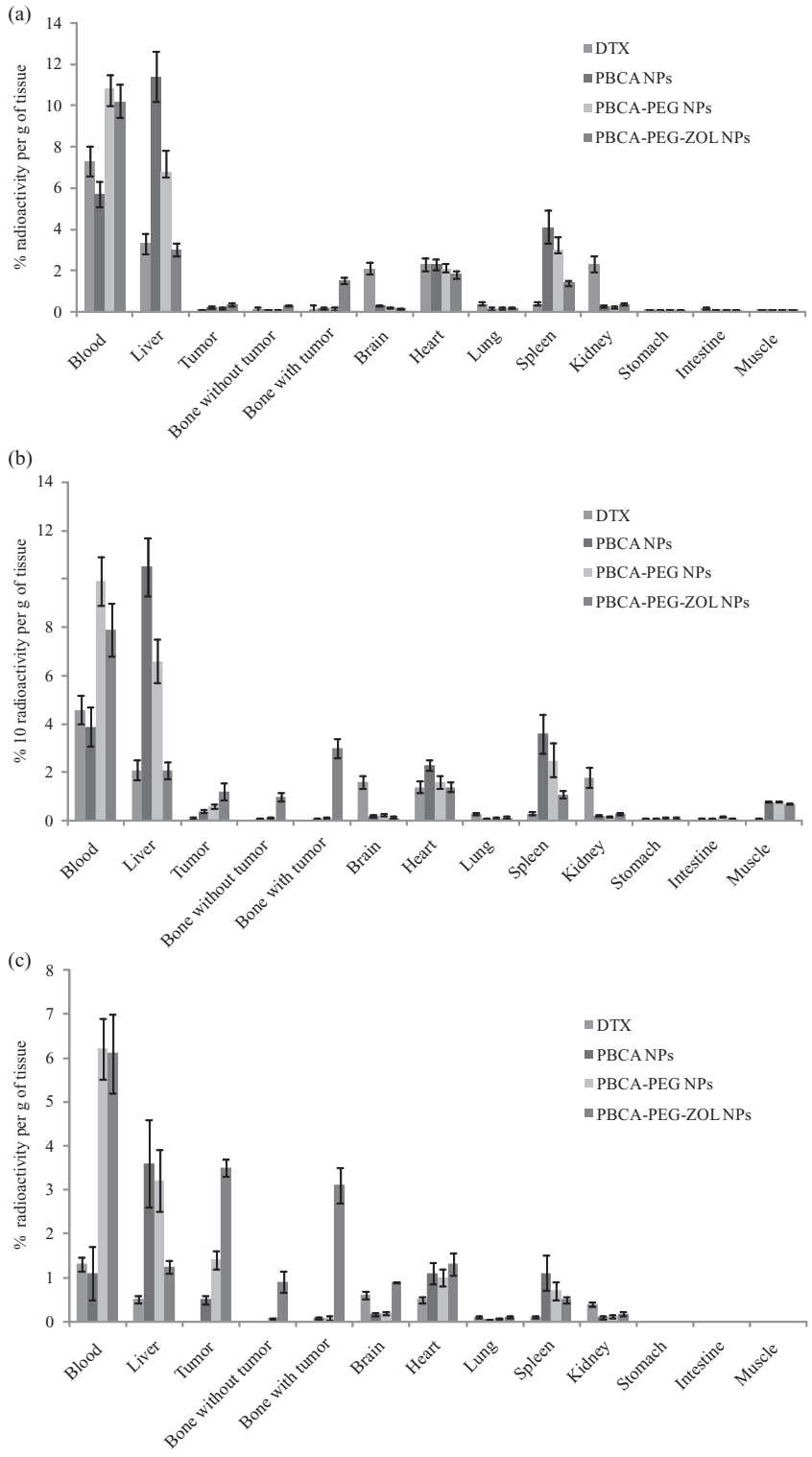

Figure 12. Biodistribution of DTX, DTX loaded PBCA NPs, PBCA-PEG NPs and PBCA-PEG-ZOL NPs using radiolabeled ^{99m}Tc-NPs complex in swiss mice. Radio activity per gram of organ/tissue was measured after a) 1 h, b) 4 h, and c) 12 h. Data presented as mean ± SEM, n = 3.

NPs accumulated largely in liver (11.4 ± 2.2 and 6.8 ± 1.4%/g), spleen (4.1 ± 0.9 and 3.0 ± 0.4%/g) and heart (2.3 ± 0.3 and 2.1 ± 0.3%/g). PBCA-PEG-ZOL NPs were largely present in liver (3.0 ± 0.2%/g). At 24 h post-injection, free DTX was largely eliminated from all the tissues. However, PBCA NPs, PBCA-PEG NPs and PBCA-PEG-ZOL NPs were accumulated in normal tissues to a higher level than free DTX. Distribution of nanoparticulate formulations in the liver was higher than free DTX at all time points (with almost 5 and 7 times more after 4 and 24 h, respectively). This might be due to penetration of NPs through fenestrae in endothelial linings of the liver associated with parenchymal cells. It has been reported by Stolnik et al. and supported by Snehalatha et al. that sterically stabilized NPs distribute mainly to the parenchymal cells after intravenous administration.[52,53]

Bone targeting affinity of PBCA-PEG-ZOL NPs was determined by the distribution at the bone bearing tumor, in comparison to non tumor bearing bone (normal bone). The ratio of NP concentration in tumor bearing bone to the normal bone was found to be 3 fold at any time point, which clearly suggests the targeting efficiency of ZOL as ligand. At the end of 24 h, the maximum amount of radioactivity was found in tumor and bone bearing tumor, as compared with other tissues. When ZOL conjugated NPs were compared with unconjugated but pegylated NPs, localization of former in tumor bearing bone significantly increased with time and found to be 7.5 ($p < 0.01$), 20 ($p < 0.001$) and 155 ($p < 0.001$) times higher after 1, 4 and 24 h respectively. This study was found in accordance with the pharmacokinetics of ZOL, which reports 40 and 50% excretion in 24 h and 6 months, respectively.[54] They confirmed that the concentration of ZOL in bone was found to be more than 100 times of plasma C_{max}, at all the tested time points. The results clearly suggest that ZOL possess more affinity towards tumor bearing bone than normal bone, in the same animal. Bone is covered with lining cells which might prevent the binding of ZOL with the bone to some degree, but during osteoporosis or bone metastasis, this lining largely gets removed due to active bone remodeling. ZOL is known to contain higher affinity towards the open bone remodeling site and thus gets accumulated and stays for longer duration of time than in normal healthy bone.[55] ZOL enhanced the targeting ability of NPs by strong affinity towards the affected bone, EPR effect, prolonged circulation half-life, as well as enhanced endocytosis. Substantial uptake in the tumor bearing bone concludes the recommendation of PBCA-PEG-ZOL NPs, for targeted and effective tumor and metastasis therapy.

4. Conclusion

Drug targeting to treat bone metastasis has been always a challenge due to the pharmacokinetic profiles of the drugs. As a result of the high affinity of ZOL towards bone, the ZOL conjugated PEGylated PBCA nanoparticles loaded with DTX were highly localized to the tumor infected bone. There was also enhanced uptake of the NPs by the tumor cells, and showed a synergistic effect on the cell cycle arrest and induction of apoptosis. Thus, ZOL conjugated NPs provide an efficient and targeted delivery of DTX with synergistic effects. These NPs may be used to facilitate highly efficient targeting of drugs, which are aimed to treat bone diseases, including bone metastasis.

Supporting Information

Supporting Information is available from the Wiley Online Library or from the author.

Acknowledgements

This research was supported by National Doctoral Fellowship from All India Council of Technical Education (AICTE) (1-10/RID/NDF-PG/(39)2008-2009), India. The authors are thankful to Evobond, Tong Shen Enterprise, Taiwan, for providing the gift sample of butylcyanoacrylate monomer. They also thank Mrs. Krishna Chuttani for her kind help in conducting animal studies, and Marjo Jauhiainen for her help with the estimation of IPP and ApppI.

Received: October 1, 2011
Revised: March 18, 2012
Published online: June 12, 2012

[1] J. M. Chirgwin, T. A. Guise, *Sci. Med.* **2003**, *9*, 140.
[2] G. R. Mundy, *Cancer* **1997**, *80*, 1546.
[3] E. C. Woodhouse, R. F. Chuaqui, L. A. Liotta, *Cancer* **1997**, *80*, 1529.
[4] A. A. El-Mabhouha, C. A. Angelov, R. Cavell, J. R. Mercer, *Nucl. Med. Biol.* **2006**, *33*, 715.
[5] H. Fleisch, *Endocr. Rev.* **1998**, *19*, 80.
[6] X. M. Liu, A. T. Wiswall, J. E. Rutledge, M. P. Akhter, D. M. Cullen, R. A. Reinhardt, D. Wang, *Biomaterials* **2008**, *29*, 1686.
[7] V. Hengst, C. Oussoren, T. Kissel, G. Storm, *Int. J. Pharm.* **2007**, *331*, 224.
[8] H. Bentz, D. Rosen, European Patent, **1992**, 0512844.
[9] M. J. Robert, A. Kozlowski, US Patent, **2002**, 6436386.
[10] T. Chen, J. Berenson, R. Vescio, R. Swift, A. Gilchick, S. Goodin, P. LoRusso, P. Ma, C. Ravera, F. Deckert, H. Schran, J. Seaman, A. Skerjanec, *J. Clin. Pharmacol.* **2002**, *42*, 1228.
[11] S. Alila, A. M. Ferraria, A. M. Botelho do Rego, S. Boufi, *Carbohydr. Polym.* **2009**, *77*, 553.
[12] K. R. Chaudhari, M. Ukawala, A. S. Manjappa, A. Kumar, P. K. Mundada, A. K. Mishra, R. Mathur, J. Mönkkönen, R. S. R. Murthy, *Pharm. Res.* **2012**, *29*, 53.
[13] O. Peyruchaud, B. Winding, I. Pecheur, C. M. Serre, P. Delmas, P. Clezardin, *J. Bone Miner. Res.* **2001**, *16*, 2027.
[14] S. K. Sahoo, V. Labhasetwar, *Mol. Pharmacol.* **2005**, *2*, 373.
[15] T. K. Jain, J. Richey, M. Strand, D. L. Leslie-Pelecky, C. A. Flask, V. Labhasetwar, *Biomaterials* **2008**, *29*, 4012.
[16] J. Panyam, V. Labhasetwar, *Pharm. Res.* **2003**, *20*, 212.
[17] F. Vega, L. J. Medeiros, V. Leventaki, C. Atwell, J. H. Cho-Vega, L. Tian, F. X. Claret, G. Z. Rassidakis, *Cancer Res.* **2006**, *66*, 6589.
[18] M. Jauhiainen, H. Mönkkönen, J. Räikkönen, J. Mönkkönen, S. Auriola, *J. Chromatogr., B: Anal. Technol. Biomed. Life Sci.* **2009**, *877*, 2967.
[19] H. Monkkonen, P. Moilanen, J. Monkkonen, J. C. Frith, M. J. Rogers, S. Auriola, *J. Chromatogr., B: Biomed. Sci. Appl.* **2000**, *738*, 395.
[20] L. H. Reddy, R. K. Sharma, K. Chuttani, A. K. Mishra, R. R. Murthy, *AAPS J.* **2004**, *6*, e23.
[21] N. Arulsudar, N. Subramanian, P. Mishra, K. Chuttani, R. K. Sharma, R. S. Murthy, *AAPS J.* **2004**, *6*, 45.
[22] G. B. Saha, *Fundamentals of Nuclear Pharmacy*, 5th ed., Springer-Verlag, New York **2005**.
[23] A. K. Babbar, A. K. Singh, H. C. Goel, U. P. S. Chauhan, R. K. Sharma, *Nucl. Med. Biol.* **2000**, *27*, 419.
[24] I. A. Khalil, K. Kogure, H. Akita, H. Harashima, *Pharmacol. Rev.* **2006**, *58*, 32.
[25] S. D. Conner, S. L. Schmid, *Nature* **2003**, *422*, 37.
[26] L. Johannes, C. Lamaze, *Traffic* **2002**, *3*, 443.
[27] K. R. Chaudhari, A. Kumar, V. K. M. Khandelwal, M. Ukawala, A. S. Manjappa, A. K. Mishra, J. Monkkonen, R. S. R. Murthy, *J. Controlled Release* **2011**, *158*, 470.
[28] M. D. Chavanpatil, J. Panyam, *J. Nanosci. Nanotechnol.* **2006**, *6*, 2651.
[29] H. Y. Nam, S. M. Kwon, H. Chung, S. Y. Lee, S. H. Kwom, H. Jeon, Y. Kim, J. H. Park, J. Kim, S. Her, Y. K. Oh, I. C. Kwon, K. Kim, S. Y. Jeong, *J. Controlled Release* **2009**, *135*, 259.
[30] M. P. Desai, V. Labhasetwar, G. L. Amidon, R. J. Levy, *Pharm. Res.* **1996**, *13*, 1838.
[31] Y. H. Kim, S. H. Gihm, C. R. Park, K. Y. Lee, T. W. Kim, I. C. Kwon, H. Chung, S. Y. Jeong, *Bioconjugate Chem.* **2001**, *12*, 932.
[32] F. C. MacLaughlin, R. J. Mumper, J. Wang, J. M. Tagliaferri, I. Gill, M. Hinchcliffe, A. P. Rolland, *J. Controlled Release* **1998**, *56*, 259.
[33] S. K. Sahoo, J. Panyam, S. Prabha, V. Labhasetwar, *J. Controlled Release* **2002**, *82*, 105.
[34] A. M. Torche, P. Le Corre, E. Albina, A. Jestin, R. Le Verge, *J. Drug Targeting* **2000**, *7*, 343.
[35] S. Blau, T. T. Jubeh, S. M. Haupt, A. Rubinstein, *Crit. Rev. Ther. Drug Carrier Syst.* **2000**, *17*, 425.
[36] J. Panyam, W. Z. Zhou, S. Prabha, S. K. Sahoo, V. Labhasetwar, *FASEB J.* **2002**, *16*, 1217.
[37] A. Catizone, L. Medolago Albani, F. Reola, T. Alescio, *Cell. Mol. Biol.* **1993**, *39*, 155.
[38] A. Rupper, J. Cardelli, *Biochim. Biophys. Acta, Gen. Subj.* **2001**, *1525*, 205.
[39] B. D. Chithrani, W. C. Chan, *Nano Lett.* **2007**, *7*, 1542.
[40] T. Mosmann, *J. Immunol. Methods.* **1983**, *65*, 55.
[41] Y. Mo, L. Y. Lim, *J. Controlled Release* **2005**, *107*, 30.
[42] N. Mondal, K. K. Halder, M. M. Kamila, *Int. J. Pharm.* **2010**, *397*, 194.
[43] D. L. Morse, H. Gray, C. M. Payne, R. J. Gillies, *Mol. Cancer Ther.* **2005**, *4*, 1495.
[44] S. A. Susin, E. Daugas, L. Ravagnan, K. Samejima, N. Zamzami, M. Loeffler, P. Costantini, K. F. Ferri, T. Irinopoulou, M. C. Prevost, G. Brothers, T. W. Mak, J. Peninger, W. C. Earnshaw, G. Kroemer, *J. Exp. Med.* **2000**, *192*, 571.
[45] S. Auriola, J. Frith, M. J. Rogers, A. Koivuniemi, J. Monkkonen, *J. Chromatogr., B: Biomed. Sci. Appl.* **1997**, *704*, 187.
[46] H. L. Benford, J. C. Frith, S. Auriola, J. Monkkonen, M. J. Rogers, *Mol. Pharmacol.* **1999**, *56*, 131.
[47] H. Monkkonen, S. Auriola, P. Lehenkari, M. Kellinsalmi, I. E. Hassinen, J. Vepsalainen, J. Monkkonen, *Br. J. Pharmacol.* **2006**, *147*, 437.
[48] J. Williams, R. Lansdown, R. Sweitzer, M. Romanowski, R. LaBell, R. Ramaswami, E. Unger, *J. Controlled Release* **2003**, *91*, 167.
[49] H. Yoshizawa, S. Nishino, K. Shiomori, S. Natsugoe, T. Aiko, Y. Kitamura, *Int. J. Pharm.* **2005**, *296*, 112.

[50] P. Ebrahimnejad, R. Dinarvand, M. R. Jafari, S. A. Tabasi, F. Atyabi, *Int. J. Pharm.* **2011**, *406*, 122.
[51] J. Park, P. M. Fong, J. Lu, K. S. Russell, C. J. Booth, W. M. Saltzman, T. M. Fahmy, *Nanomedicine: NBM.* **2009**, *5*, 410.
[52] S. Stolnik, C. R. Heald, J. Neal, M. C. Garnett, S. S. Davis, L. Illum, S. C. Purkis, R. J. Barlow, P. R. Gellert, *J. Drug Targeting* **2001**, *9*, 361.
[53] M. Snehalatha, K. Venugopal, R. N. Saha, A. K. Babbar, R. K. Sharma, *Drug Delivery* **2008**, *15*, 277.
[54] T. Chen, J. Berenson, R. Vescio, R. Swift, A. Gilchick, S. Goodin, P. LoRusso, P. Ma, C. Ravera, F. Deckert, H. Schran, J. Seaman, A. Skerjanec, *J. Clin. Pharmacol.* **2002**, *42*, 1228.
[55] J. E. Shea, S. C. Miller, *Adv. Drug Delivery Rev.* **2005**, *57*, 945.